Chapter 4

Fluoride sensing study of bis-thiourea based tweezers in aqueous medium

4.1. Introduction

Urea and thiourea-based sensors have gained considerable attention due to their exceptional selectivity and sensitivity toward fluoride and acetate ion. The easier synthetic method and facile incorporation in different scaffold make urea/thiourea motif popular in designing of new anon host in host guest chemistry. The robust H- bonding interactions between thiourea, NH and fluoride ions make them an exemplary candidate for fluoride detection [1-8]. The binding mechanism of urea/thiourea moiety with strongly basic anions in organic medium involve H-bonding followed by deprotonation of the -NH moiety. To achieve better selectivity and binding affinity researchers have used the concept of pre-organization in designing the urea/thiourea based probe for selective recognition of fluoride over acetate ion. The increase in the number of binding site as well as introduction of size constraint in the binding domain is also a noteworthy strategy for selective recognition of smaller anions like fluoride over larger anions like acetate. Building upon this foundation, researchers have developed *bis*-thiourea tweezer molecules, which incorporate two thiourea units connected by a linker which are strategically positioned within a tweezer head providing size constraint as supplementary aspects for improving anion/cation selectivity. When incorporated into a tweezer-like structure, the two thiourea arms are positioned such that they can interact synergistically with an anion positioned between them. This dual interaction is presumed to enhance the overall binding affinity and selectivity, making *bis*-urea/thiourea tweezers highly effective anion receptors. In addition to selectivity, the sensitivity of *bis*-thiourea tweezers is a significant attribute that makes them suitable for detecting anions at very low concentrations. The strong hydrogen bonds and electrostatic interactions between the thiourea groups and the anion ensure a high binding affinity, which translates to the ability to detect anions even in trace amounts. This high sensitivity is particularly vital attribute in environmental monitoring, where detecting low levels of pollutants is crucial, and in medical diagnostics, where precise quantification of physiological anions can be critical for disease diagnosis and management. Furthermore, the *bis*-thiourea/urea receptors are also explored in cation binding study where metal binding facilitated through thiourea S/urea O along with other metal coordinating site introduced in the receptor (Figure 4.1) [9-12].
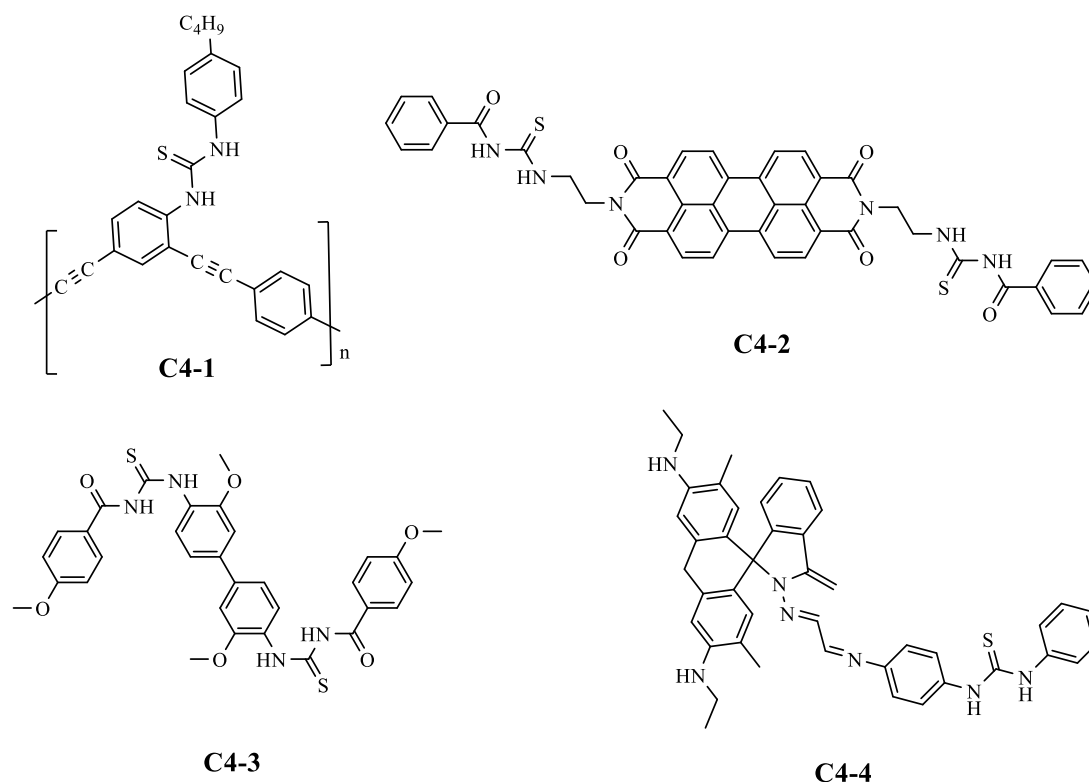
Figure 4.1: Literature report of some (Thio)urea-based molecules for metal ion sensing [9-12].

By varying the size, shape, and electronic properties of the tweezer arms, receptors with binding sites that preferentially interact with particular anions can be designed. For instance, the inclusion of electron-withdrawing or electron-donating groups can enrich or diminish the hydrogen-bonding ability of the thiourea moieties, thereby fine-tuning the selectivity [13-18]. Additionally, the spatial arrangement of the thiourea groups can be optimized to match the geometric and binding characteristics of the target anion by changing the proper functionalization and controlling the environment like solvent. By attaching various functional groups to the tweezer scaffold, the solubility, stability of the sensors can be improved. Beyond their superior binding characteristics, *bis* -thiourea tweezers can be functionalized to exhibit distinct optical and electrochemical responses upon fluoride binding [13,15,18,20]. The capability to detect fluoride ions through multiple modes of analysis further underscore the utility of *bis* -thiourea tweezers as a versatile and efficient fluoride sensor. Some of the literature reported *bis* -thiourea moieties and their fluoride binding behaviour are depicted in Table 4.1.
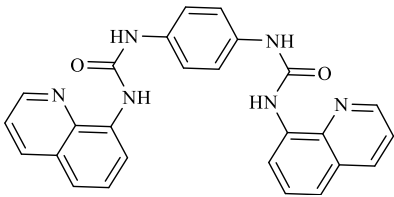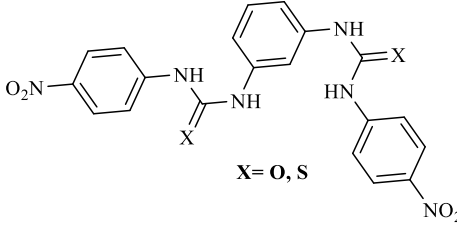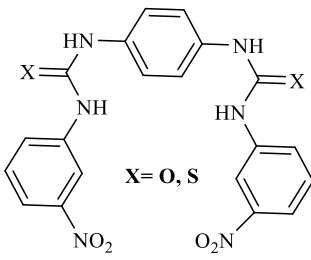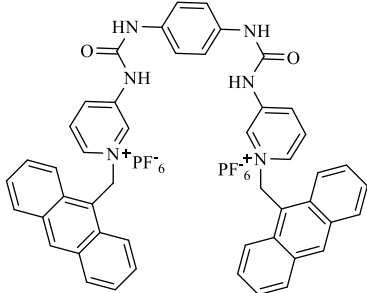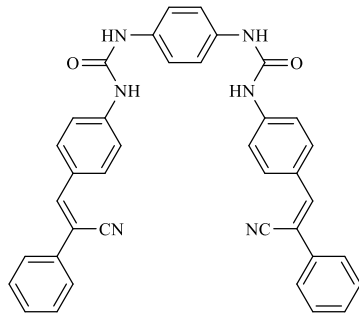
Probe	Fluoride salt used	Solvent of study	Types of sensor	References
	TBAF as F⁻ ion source	DMSO	Chromogenic	[19]
	TBAF as F⁻ ion source	DMSO	Chromogenic	[20]
	TBAF as F⁻ ion source	CH₃CN	Chromogenic	[21]
	TBAF as F⁻ ion source	CH₃CN	Chromogenic	[22]
	TBAF as F⁻ ion source	DMSO	Chromogenic	[23]

Table 4.1: Literature report of some (Thio)urea-based molecules for fluoride ion sensing.

Although *bis*-thiourea probe molecules have shown promising results with low detection values, all detections were conducted in organic media and with fluorides having organic counter ion like tetrabutylammonium ion. Their sensing ability decreases with even in the presence of small amount of water and completely fails to detect inorganic fluoride like NaF. The failure to sense fluoride ion in water is because of the relatively lower basic nature of fluoride and lower acidic nature of thiourea -NHs in water. This might be due to the lower stability of conjugate base, *i.e.*, deprotonated thiourea in water relative to the organic medium. In this chapter, we demonstrated the metal mediated strategy with the presumption that suitable metal ion would stabilise the fluoride induced conjugate base of the *bis*-thiourea receptors which eventually enable the fluoride sensing ability in aqueous medium. In this chapter we have chosen two analogues thiourea based tweezers (**S1 & S2**) to explore the metal mediated strategy (hypothesis 1) (Figure 4.2). In probe molecule **S2**, one -NH is replaced by Sulphur to see the role of the number of -NH unit in the fluoride sensing performance of the probe molecule.
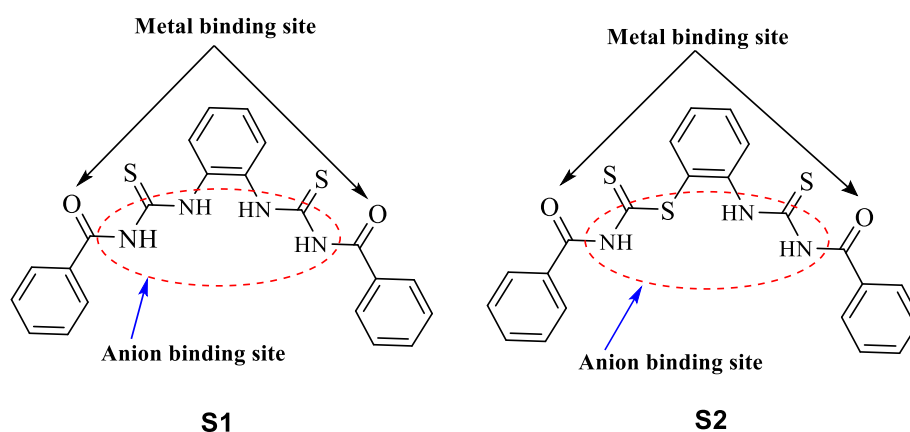

Figure 4.2: Structure of probe molecules **S1** & **S2**.

4.2. Objective of the study

The objective of the study discussed in this chapter are:

- Study the fluoride sensing affinity of two thiourea based tweezers **(S1 & S2)** in aqueous medium by following the metal mediated strategy (hypothesis 1).

- Demonstration of the methodology with UV-Visible spectroscopy and electrochemical techniques like cyclic voltammogram and differential pulse voltammetry.

- Validation of the methodology with real-life samples.

4.3. Results and discussion

4.3.1 Synthesis and Characterization

The synthesis of the receptor **S1** & **S2** is performed by following scheme 4.1 and 4.2.
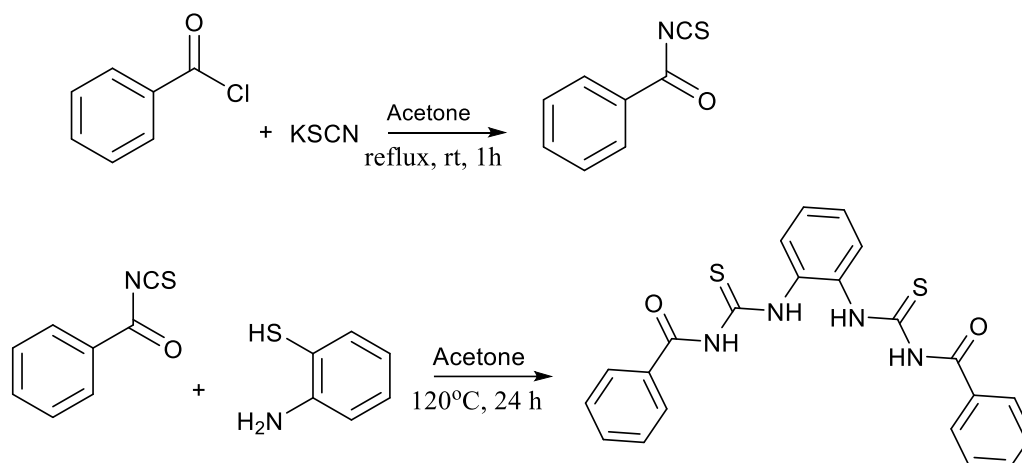
Scheme 4.1: Synthesis of **S1**.

Synthesis of S1

0.925 mmol of Potassium thiocyanate was dissolved in 15 mL acetone. To it, 0.925 mmol of the Benzoyl chloride was added dropwise with constant stirring. The mixture was then refluxed at 55°-60 °C for 1 h, cooled and filtered. To the filtrate, *o*-Phenylenediamine (0.925 mmol) dissolved in acetone was added dropwise with constant stirring. The mixture was then refluxed for another 24 h at 120° C and thereafter acetone was removed by distillation. The crude product was washed with cold water and ethanol, and dried in air.

Cream white solid, Yield: 62%, FT-IR of **S1** (cm⁻¹): υ(N-H) = 3401, υ(C=O) = 1673 and υ(C=S) = 1530. ^{1}H NMR (400 MHz, CDCl$_3$) δ 12.35 (s, 2H), 9.21 (s, 2H), 7.93 (m, *J* = 5.9, 3.6 Hz, 2H), 7.87 – 7.82 (m, 4H), 7.65 – 7.60 (m, 2H), 7.52 – 7.42 (m, 6H). ^{13}C NMR (101 MHz, CDCl$_3$) δ 180.10, 166.78, 133.69, 133.11, 131.65, 129.13, 128.14, 127.64, 126.93. LCMS (M+H) =435.10 (Calculate: 435.09).
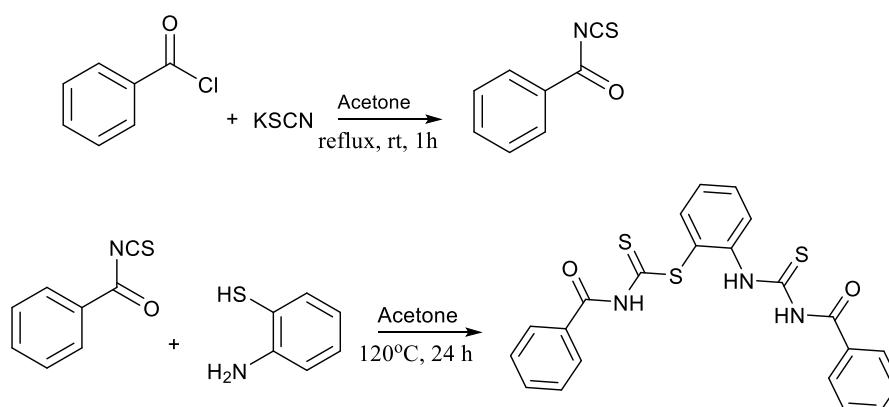
Synthesis of S2

0.925 mmol of Potassium thiocyanate was dissolved in 15 mL acetone. To it, 0.925 mmol of the Benzoyl chloride was added dropwise with constant stirring. The mixture was then refluxed at 55°-60 °C for 1 h, cooled and filtered. To the filtrate, *2*-aminothiophenol (0.925 mmol) dissolved in acetone was added dropwise with constant stirring. The mixture was

then refluxed for another 24 h at 120 ˚C and thereafter acetone was removed by distillation. The crude product was washed with cold water and ethanol, and dried in air.

Scheme 4.2: Synthesis of **S2**.

Light Yellow solid, Yield: 65%, FT-IR of **S2** (cm^{-1}): υ(N-H) = 3401, υ(C=O) = 1673 and υ(C=S) = 1530. ^{1}H NMR (400 MHz, CDCl$_3$) δ 12.55 (s, 1H), 10.37 (s, 1H), 9.16 (s, 1H), 8.46 – 8.37 (m, 1H), 8.00 – 7.95 (m, 2H), 7.81 – 7.78 (m, 2H), 7.70 – 7.52 (m, 7H), 7.50 – 7.44 (m, 3H).^{13}C NMR (101 MHz, CDCl$_3$) δ 202.27, 179.05, 166.53, 163.85, 140.91, 136.42, 133.66 (d, J = 9.9 Hz), 131.45, 129.20, 129.06, 128.01 (d, J = 2.2 Hz), 127.59, 126.79. LCMS (M+H) =451.05 (Calculate: 451.04).

Crystal structure analysis of S1 and S2

Single crystals of both receptors were generated through solution crystallization by slow evaporation of the solvent, resulting in two polymorphic forms of **S1**. Single crystals of **S1** obtained from ethanol (hereafter termed **Form 1**) were solved in the triclinic $P\bar{1}$ space group, containing one molecule in the asymmetric unit (Appendix A 2.2, table A2.2). Structural analysis reveals a tweezer-type conformation with two intramolecular N–H···O hydrogen bonds between the two independent thiourea N–H functionals and the benzoyl carbonyl moieties. No strong intermolecular H-bonding have been observed between the neighbouring molecules. In 3D, one of the tweezer arms stacks over neighbouring molecules via π···π interactions between the terminal benzene ring and the thiourea moiety, as shown in Figure 4.3. During attempted complexation with nickel salt, another polymorphic form of **S1** was obtained (hereafter designated as **Form 2**), also solved in the triclinic $P\bar{1}$ space group. Structural analysis of Form 2 depicted two independent molecules in the asymmetric unit. Similar to Form 1,

S1 (Form 1)   **S1 (Form 2)**

(a)   **(d)**

(b)   **(e)**

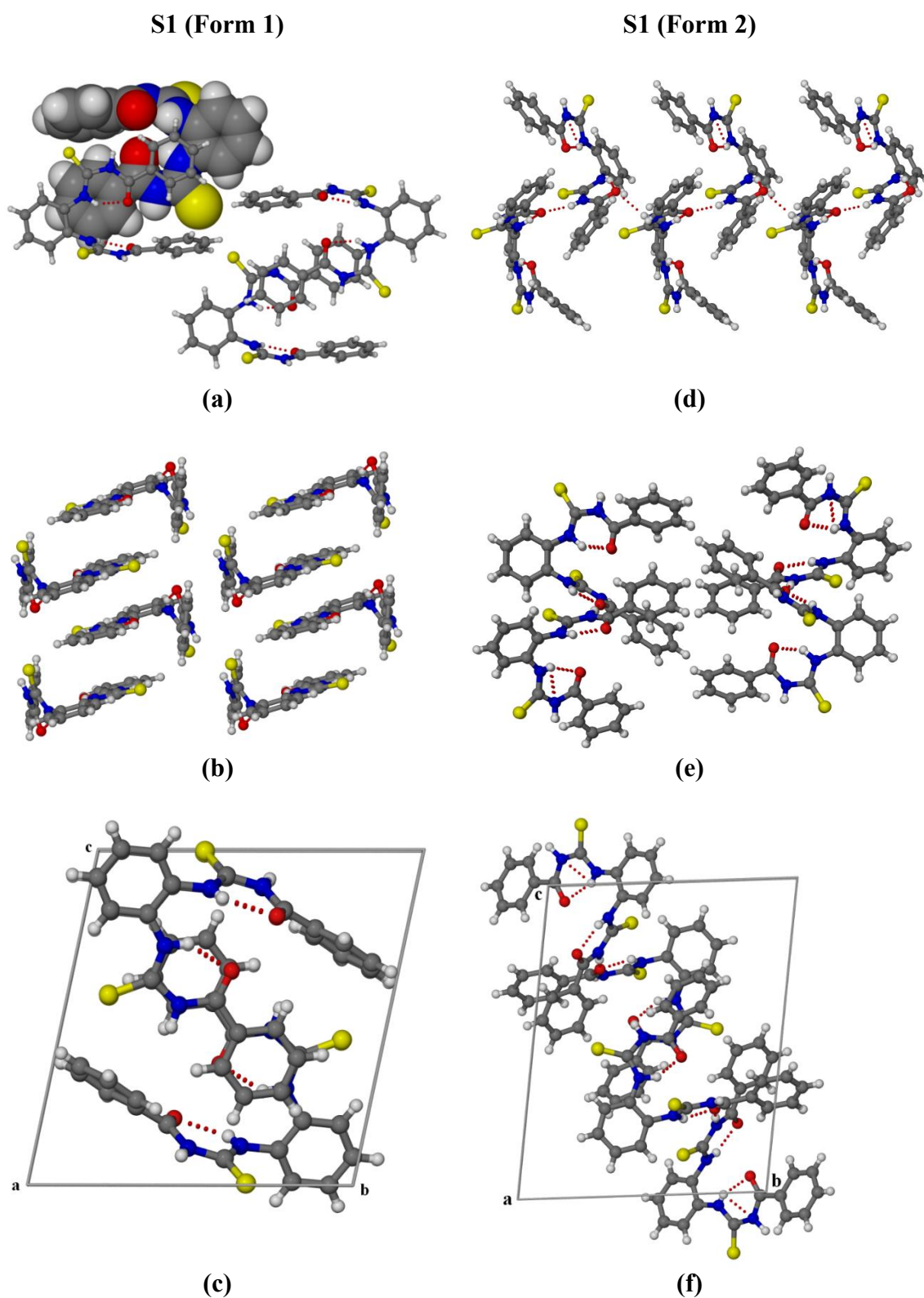**(c)**   **(f)**

Figure 4.3: (a, b, c) $\pi\cdots\pi$ stacking arrangement of **S1** molecule in Form I resulting the 3D packing arrangement; (d, e, f) an interdigitated infinite chain is formed using N–H$\cdots$O hydrogen bond between symmetry independent **S1** molecules in Form 2.

Form 2 also have two intramolecular N–H···O hydrogen bonds between the thiourea and carbonyl moieties. In 3D, the two independent molecules are further interacted by N–H···O hydrogen bonds between the N–H and carbonyl groups of neighbouring units, forming an infinite chain along the *a*-axis. Interdigitated parallel chains result in the 3D packing arrangement, as shown in Figure 4.3. SCXRD structure of **S2** revealed the presence of intramolecular interstrand N–H···O hydrogen bonding, along with the interpenetration of one arm in the cleft of another **S2** through π-π interaction, dictating the 3D packing.

4.3.2. Anion affinity Study of S1 and S2 in Organic Medium

The preliminary anion affinity of the probe molecules in dimethyl sulfoxide (DMSO) medium was analysed using UV−Vis spectroscopy. The UV−Vis spectra of the colourless solutions of both **S1** and **S2** in DMSO showed absorbance at 270 nm and 290−320 nm,
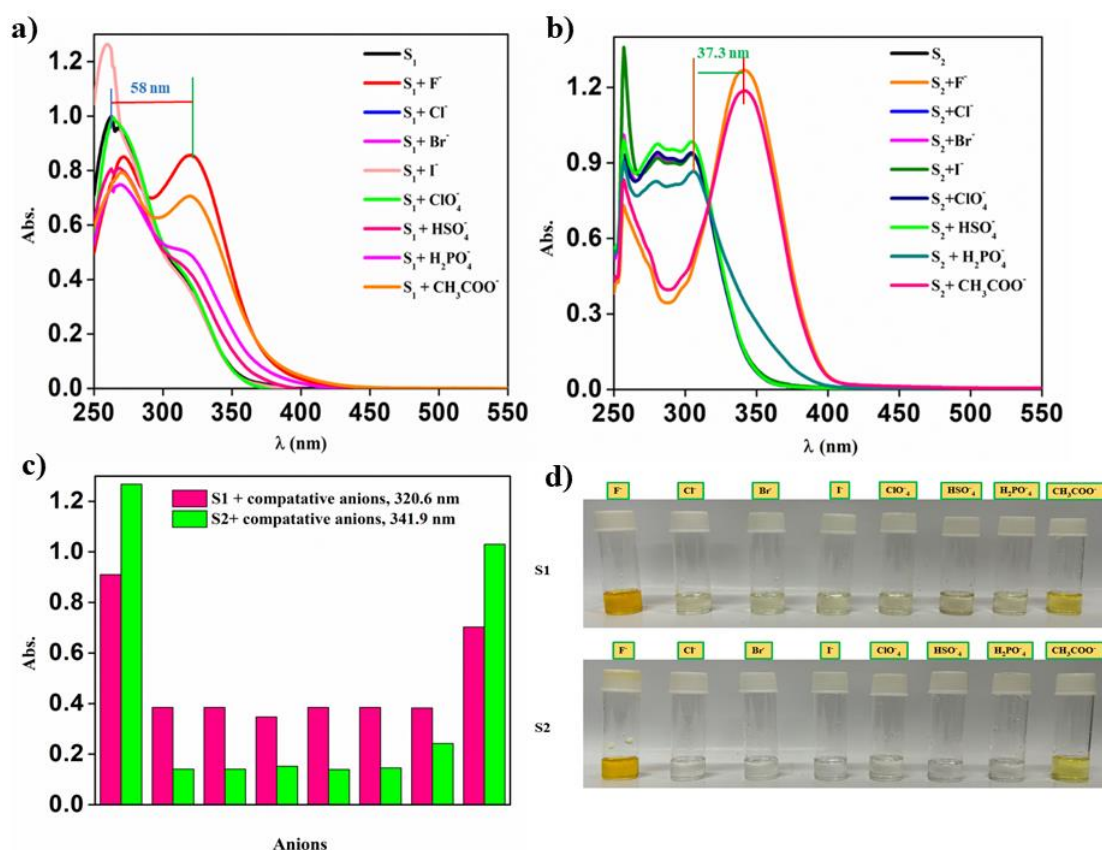
Figure 4.4: (a) UV-Vis spectra of **S1** in DMSO (6×10^{-5} M) upon addition of anions in DMSO; (b) UV-Vis spectra of **S2** in DMSO (6×10^{-5} M) upon addition of anions in DMSO; (c) Bar diagram showing changes in the absorbance of **S1** (Pink) and **S2** (Green) in DMSO (both 6×10^{-5} M concentration) upon addition of different anion solutions (5×10^{-2} M); (d) Colorimetric changes upon addition of anions to **S1** and **S2**.
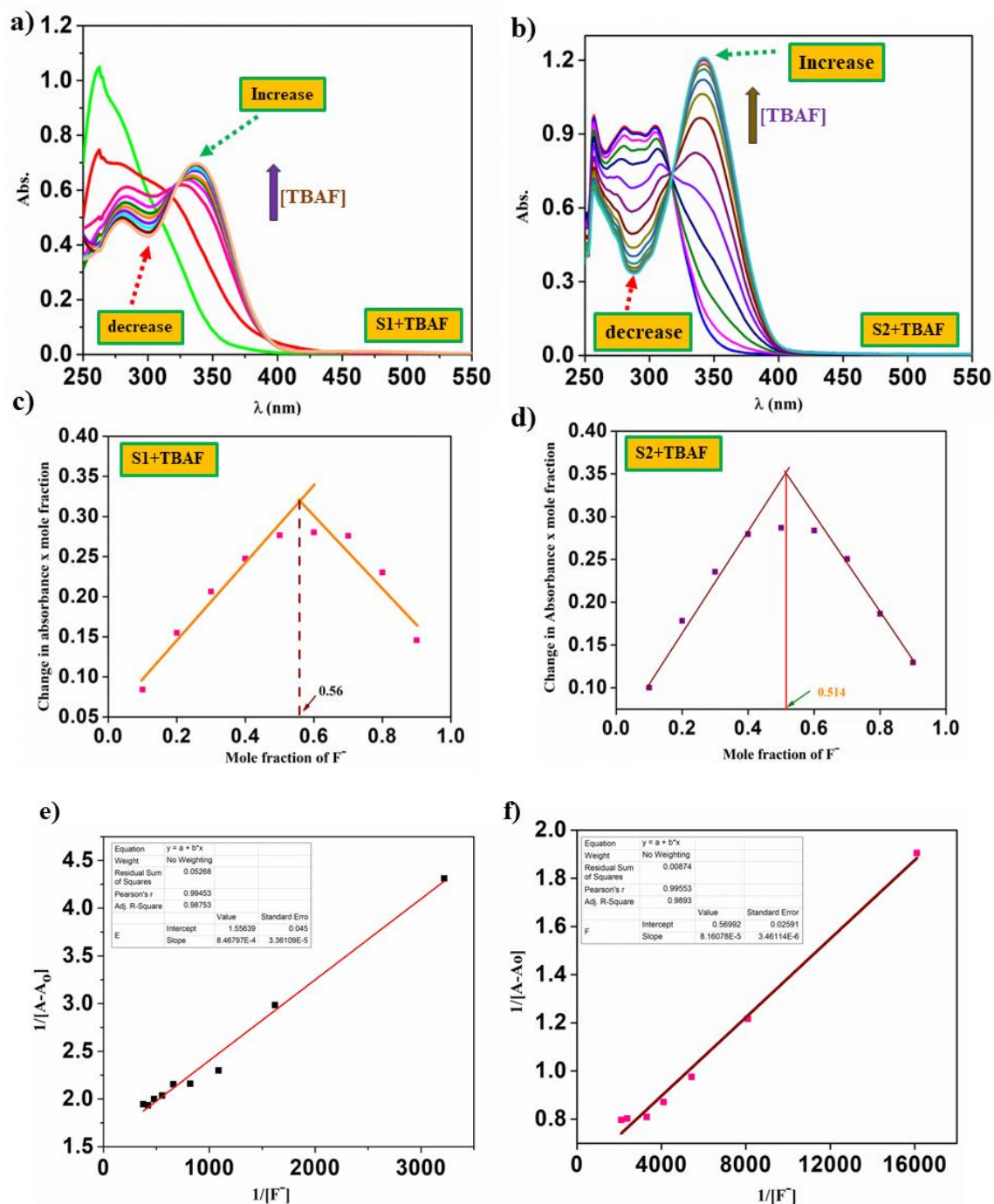
Figure 4.5: (a) UV-Vis spectra of **S1** in DMSO (6×10^{-5} M) upon gradual addition of TBAF (10×10^{-3} M) in DMSO; (b) UV-Vis spectra of **S2** in DMSO (6×10^{-5} M) upon gradual addition of TBAF (10×10^{-3} M) in DMSO ; (c) Job's plot of **S1** representing 1:1 stoichiometric interaction between **S1** and F^-; (d) Job's plot of **S2** representing 1:1 stoichiometric interaction between **S2** and F^-; (e) Benesi-Hildebrand plot of **S1**.F^- interaction; (f) Benesi-Hildebrand plot of **S2**.F^- interaction.

respectively. The anion binding affinity of the tweezers (**S1** and **S2**) was studied by monitoring the changes in the UV−Vis spectrum of the probe solution in DMSO (6×10^{-5} M) upon addition of tetrabutylammonium salts of various anions (F^-, Cl^-, Br^-, I^-, ClO_4^-, HSO_4^-, $H_2PO_4^-$, and CH_3COO^-). Both receptors showed affinity towards fluoride and acetate anions, evidenced by the colour change of the solution to yellow (Figure 4.4).Upon interaction with F^- and CH_3COO^- ions, probe **S1** displayed a new sharp peak at 340 nm. Similarly, **S2** in DMSO solution exhibited the emergence of the peak at 370 nm upon addition of F^- and CH_3COO^- ions (Figure 4.4). The colour change is more distinct with fluoride compared to acetate for both **S1** and **S2**. Titration of **S1** with fluoride ions in DMSO revealed a lowering of the intensity of absorbance at 270 nm, accompanied by a concomitant increase in the absorbance at 340 nm. Likewise, **S2** displayed a continuous

Figure 4.6: UV-Vis spectra of probe molecules and F^- mixture in DMSO upon addition of water with corresponding colorimetric 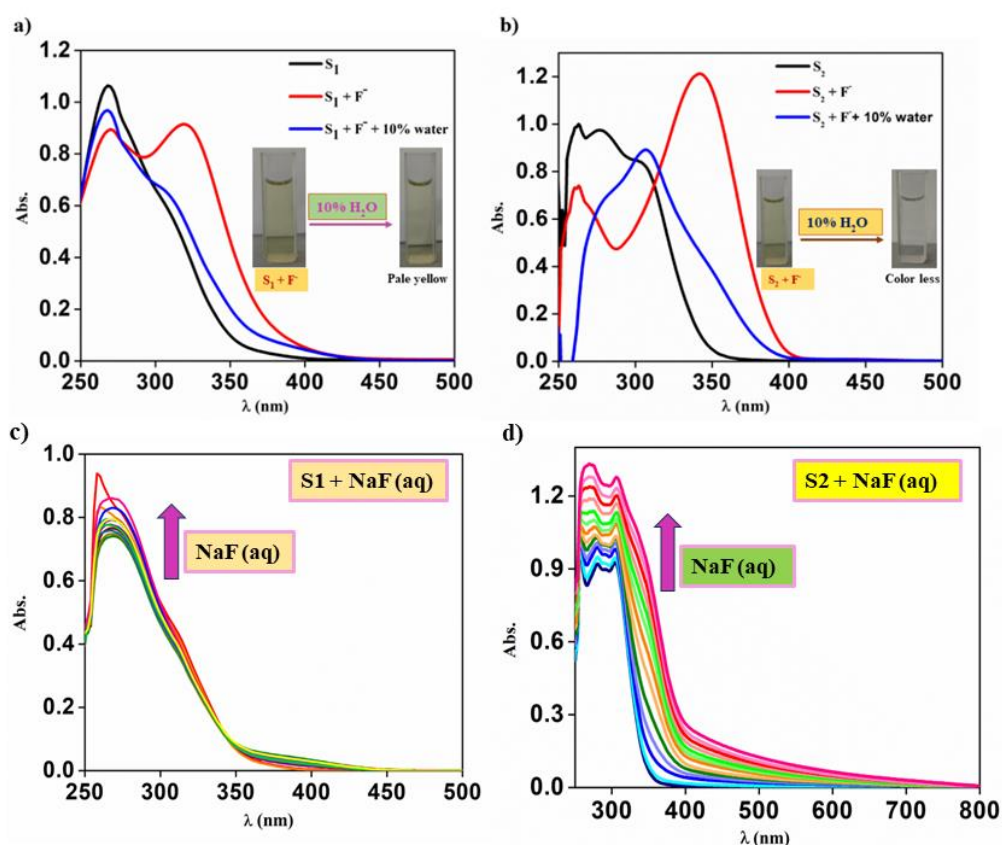change (a) **S1**.F^- and (b) **S2**.F^-; (c) UV-Vis spectra of **S1** in DMSO (6×10^{-5} M) upon gradual addition of NaF (10×10^{-3} M) in water; (d) UV-Vis spectra of **S2** in DMSO (6×10^{-5} M) upon gradual addition of NaF (10×10^{-3} M) in water.

decrease in the intensity of the broad peak at 290−320 nm, with simultaneous increase in the intensity of the peak at 370 nm, maintaining an isosbestic point at 335 nm (Figure 4.5b). Job's plot analysis indicated the plateau at 0.5, suggesting a 1:1 stoichiometry for the interaction of **S1** and **S2** with fluoride ion (Figure 4.5 c,d). The binding constants for the interaction of the probe molecules with F⁻ were calculated using the Benesi−Hildebrand plot, yielding values of 1.83×10^3 M⁻¹ and 6.89×10^3 M⁻¹, respectively (Figure 4.5 e,f). After demonstrating the fluoride affinity of both **S1** and **S2** in organic medium, their affinity towards aqueous fluoride ions was investigated by adding 300 µL of 10% (V/V) water to the solution of **S1** · F⁻ and **S2** · F⁻ in 3 mL of DMSO (Figure 4.6 a,b). It was observed that the solution's colour become faded, and the distinctive absorbance of the peak in the visible region diminished. Furthermore, the addition of an aqueous NaF solution to the probe solutions (**S1** and **S2**) did not show any remarkable effect on the UV−Vis spectra, indicating their inability to interact with fluoride ions in presence of water (Figure 4.6 c,d).

4.3.3. ¹H-NMR titration study

To understand the mode of interaction between the probe molecule and the fluoride ion, ¹H NMR titration experiment was conducted. Upon addition of fluoride ion to **S1** in DMSO-d_6 medium, the signals at 12.5 and 11.75 ppm corresponding to the thiourea N−Hs, initially broadened, and nearly disappeared with the addition of 1.5 equivalents of fluoride. Further increase in the fluoride concentration led to the disappearance of the signals at 12.21 and 13.65 ppm, with subsequent appearance of a new broad peak at 16 ppm, corresponding to the HF₂⁻ ion (Figure 4.7a). Surprisingly, some of the phenyl ring protons shifted up-field, indicating an increase in electron density in the phenylenediamine unit, while others shifted downfield, indicating a decrease in electron density in the benzoyl phenyl moiety upon interaction with fluoride. These observations suggest partial deprotonation of the N−H protons by the fluoride ion, as the remaining two N−Hs are involved in intramolecular H-bonding with the carbonyl oxygen of the benzoyl moiety. Consequently, the ¹H NMR study suggests that the recognition of fluoride by the probe molecule **S1** involves a Bronsted acid−base deprotonation reaction, potentially creating favourable coordination sites for Ni(II) complexation. This observation was further confirmed by ¹⁹F-NMR, which shows sharp peak at -145 ppm indicating the formation of HF₂⁻ (Figure 4.7b).
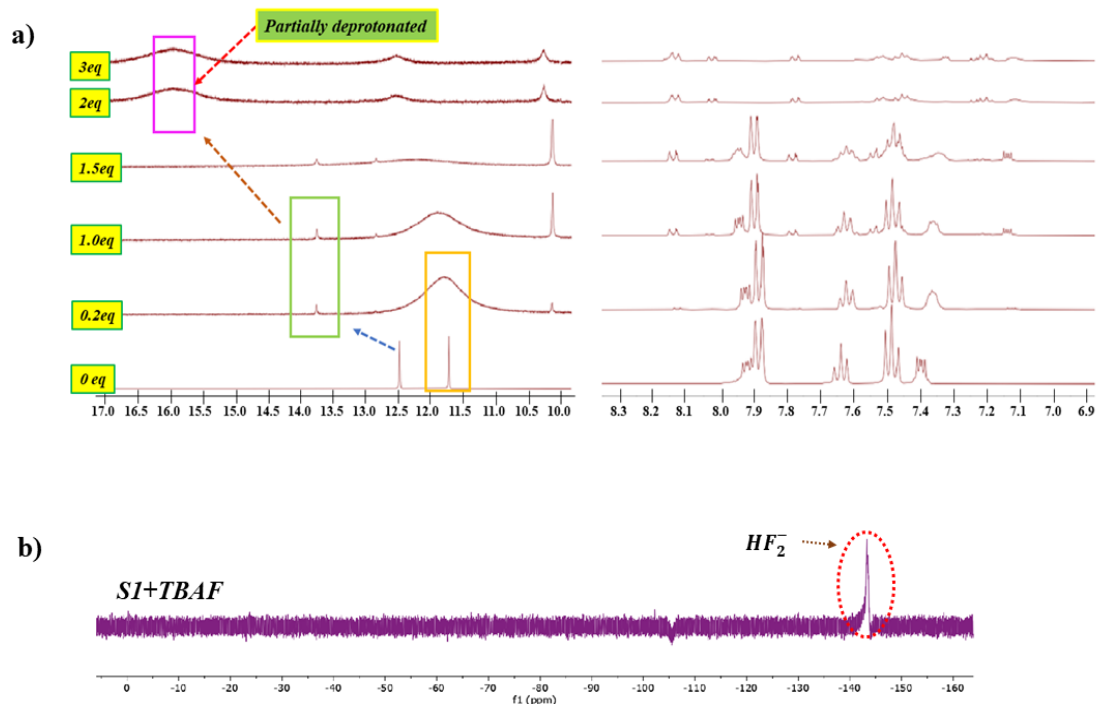
Figure 4.7: (a) Change in the ^{1}H NMR signals of receptor **S1** in DMSO-d_6 upon addition of fluoride ion; (b) ^{19}F NMR of TBAF titration to probe **S1.**

4.3.4. Fluoride recognition study of S1 and S2 in aqueous medium

4.3.4.1. UV-Vis spectroscopy study

To develop a strategy for making the colorimetric response of the studied tweezers toward the fluoride ion persistent in the water medium, we examined the deprotonation equilibrium of the probe molecules with aqueous fluoride ions in presence of transition metal ions. It was anticipated that in situ transition metal complexation might enhance the colorimetric sensing response by improving the colorimetric change through metal-to-ligand or ligand-to-metal charge transfer (LMCT) transitions. In this study, metal salts that do not show any affinity toward the probe molecules (**S1** and **S2**) in the absence of fluoride ions were
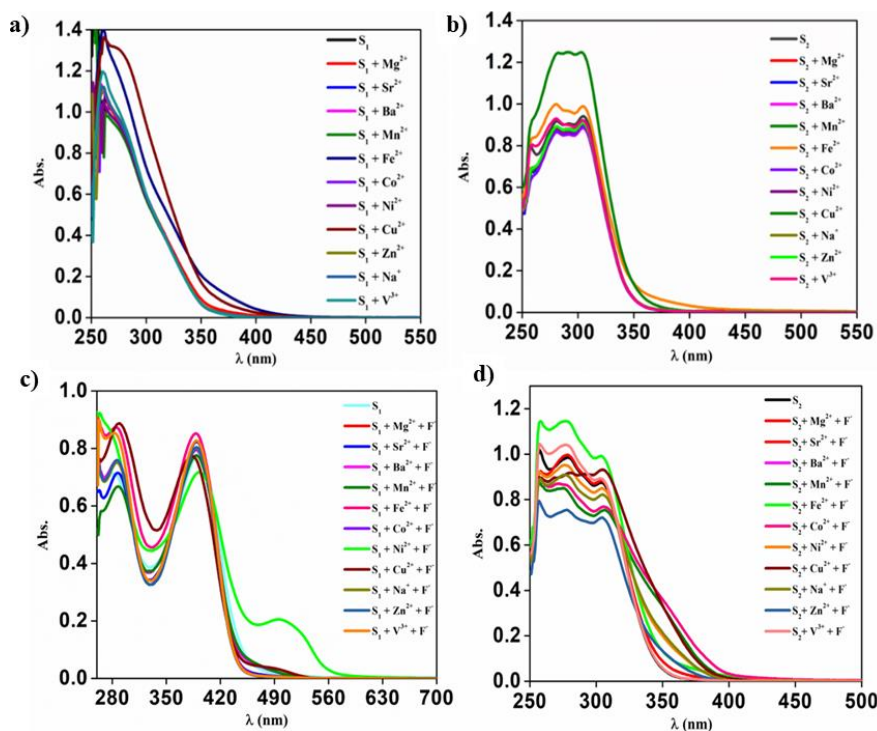
Figure 4.8: UV-Vis absorbance of the probe molecule [6×10^{-5} M] in DMSO solution upon addition of different metal salts [10×10^{-3} M] (NaCl, MgSO$_4$, VCl$_3$, MnCl$_2$, FeCl$_2$, FeCl$_3$, CoCl$_2$, NiCl$_2 \cdot 6H_2O$, CuCl$_2 \cdot 2H_2O$, ZnCl$_2$, SrCl$_2$, BaSO$_4$): (a) **S1** in absence of F$^-$ ion; (b) **S1** in presence of F$^-$ ion; (c) **S2** in absence of F$^-$ ion and (d) **S2** in presence of F$^-$ ion.

considered suitable for the purpose. Chloride and sulphate salts of the metal ions were chosen, as both probe molecules did not show any affinity for these counter anions. The affinity of both probe molecules toward metal ions was investigated by monitoring the UV−Vis spectrum of **S1** and **S2** solutions in DMSO (6×10^{-5} M) by adding a 10 mM aqueous solution of the following metal salts: NaCl, MgSO$_4$, VCl$_3$, MnCl$_2$, FeCl$_2$, FeCl$_3$, CoCl$_2$, NiCl$_2 \cdot 6H_2O$, CuCl$_2 \cdot 2H_2O$, ZnCl$_2$, SrCl$_2$, and BaSO$_4$. It was found that neither **S1** nor **S2** showed any affinity for the tested metal salts (Figure 4.9 a,b). Subsequently, the UV−Vis spectrum of **S1** and **S2** in DMSO was recorded after adding metal salt solutions and an aqueous solution of fluoride (10×10^{-3} M). It was observed that addition of Ni (II) salt to the **S1.F$^-$** solution in DMSO altered the colour of the solution from colourless to red. However, no substantial colour change was observed upon the addition of other aqueous metal salt solutions to **S1** in the presence of fluoride (Figures 4.9 a,b). Reversing the order of addition of Ni(II) salt and aqueous fluoride salt solution to **S1** produced a similar colorimetric output. Similarly, the fluoride binding affinity of **S2** in the aqueous medium
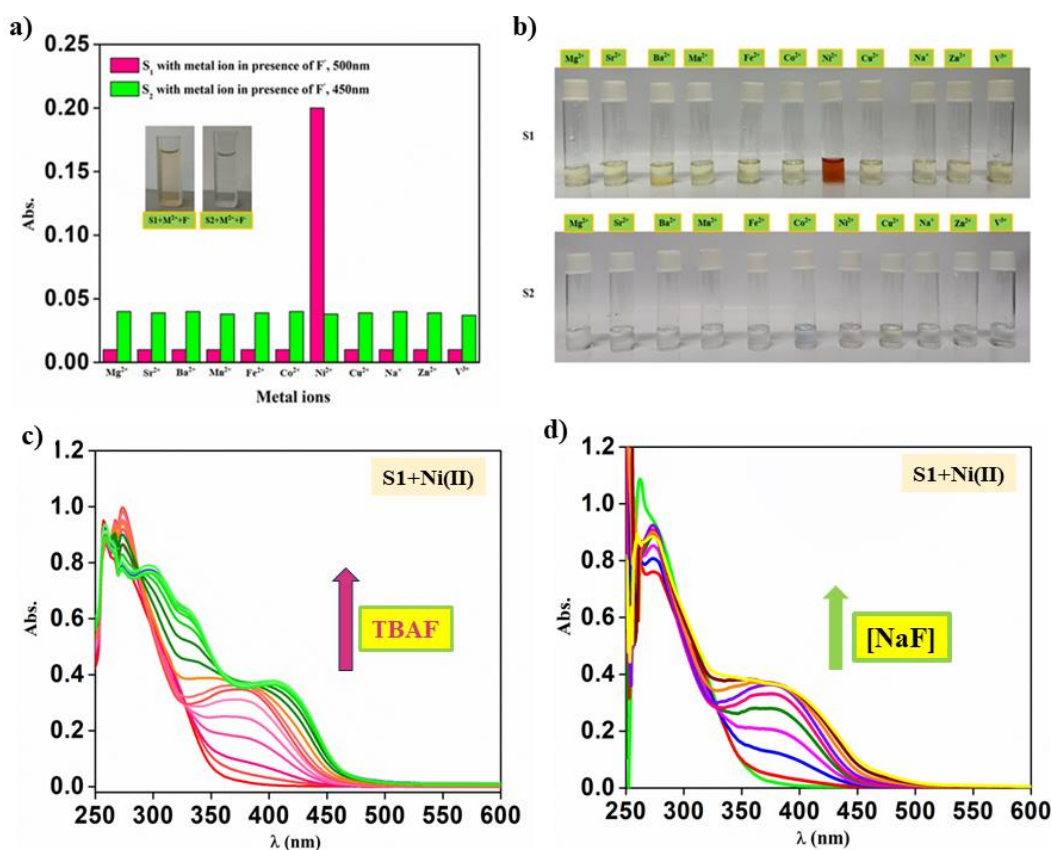
Figure 4.9: (a) Bar representation of the change in absorbance of **S1** [6×10^{-5} M] in DMSO solution upon addition of different metal salts [10×10^{-3} M] as aqueous solution in presence of F$^-$ ion; (b) Colorimetric change of S1 and S2 solution in presence of fluoride and added metal salts; (c) Change in UV-Vis spectra of **S1** [6×10^{-5} M] in DMSO upon gradual addition of TBAF(DMSO) in presence of Ni(II) ion; (d) Change in UV-Vis spectra of **S1** [6×10^{-5} M] in DMSO upon gradual addition of NaF(aqueous) in presence of Ni(II) ion.

was also tested in the presence of different metal salts. However, **S2** did not show any significant response toward the fluoride ion in water medium, even in the presence of metal ions (Figure 4.9d). This observation suggested that among the two studied probe molecules, **S1** has the potential to be used as a probe for sensing fluoride ions in water medium in presence of NiCl$_2$ salt. Therefore, compound **S1** was considered suitable for further study. Gradual addition of an aqueous solution of TBAF to **S1**.Ni(II) solution in a DMSO-H$_2$O mixture led to gradual evolution of the peak at λ_{max} 380 nm and at λ_{max} 430 nm by maintaining two isosbestic point at 340 nm and 380 nm, respectively, indicating the involvement of two processes, *i.e.*, deprotonation and Ni(II) complexation. On the same note, titration of **S1**.Ni(II) solution in DMSO-H$_2$O medium with NaF(aq) solution led to

the emergence of the broad peak at 330−450 nm, whose intensity increases with the addition of NaF (Figure 4.9 c,d). Furthermore, it was observed that 0.3 ppm aqueous fluoride can lead to an appreciable change in the UV−Vis spectrum of **S1** in the presence of Ni(II) salt (Figure 4.9a). The UV-Vis experiments clearly demonstrated that the probe molecule **S1** can serve as a colorimetric sensor for fluoride ions in an aqueous medium when Ni(II) ions are present. The optimum concentrations of **S1** and NiCl$_2$ to be used in the detection of the fluoride ion in water medium is determined and found as the mixture of 3 mL solution of **S1** (6.7×10^{-5} M) in DMSO and 50 μL solution of NiCl$_2$ (10 mM) in water. The change in absorbance at 380 nm peak of the probe solution [**S1**and Ni (II) in DMSO−H$_2$O mixture] fitted linearly with increase in the concentration of the fluoride ion (Figure 4.10). The limit of detection was calculated for the probe molecule **S1** in the presence of Ni(II) and found to be to be 0.2 ppm [23]. It is found that the red colour of the reaction mixture (**S1** (DMSO) + Ni^{2+}(aq) + NaF(aq)] as well as the UV-Vis absorption peak remained persist upon incremental addition of water (Figure 4.11a) However, the colorimetric observation that occurs after adding F$^-$ to the **S1** solution in DMSO in absence of Ni (II) diminished upon addition of water. This study clearly inferred the formation of stable Ni(II) complex of **S1** in aqueous medium. Furthermore, Al^{3+} and Fe^{3+}, which are
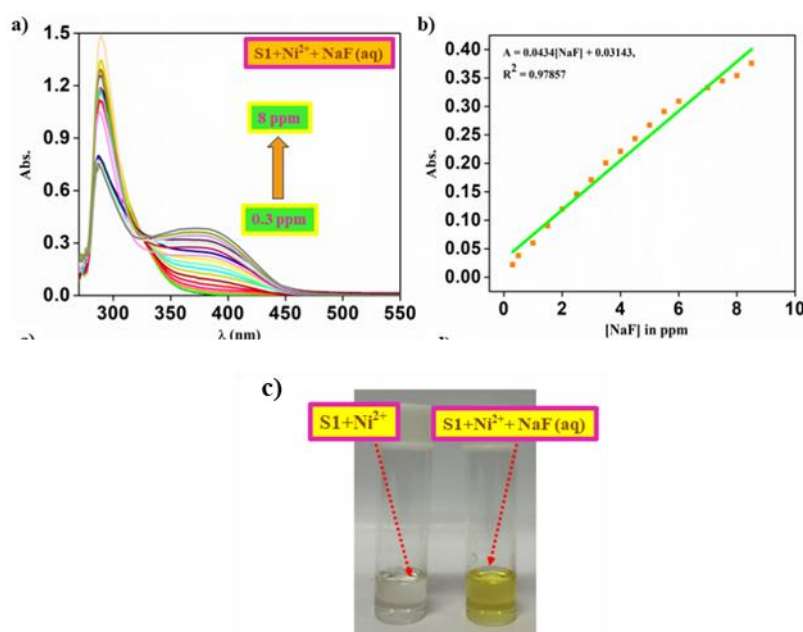

Figure 4.10: (a) UV-Vis absorbance of **S1** [6×10^{-5} M] in DMSO upon gradual addition of NaF(aq) in ppm level in presence of Ni (II) ion; (b) Calibration curve of the above; (c) Colorimetric changes upon addition of NaF in ppm.

typically the most potential interfering ions in the SPADNS and ion selective method, did not show any significant change in the colorimetric response of this strategy. Furthermore, in contrast to the observation in DMSO medium with organic anions, **S1** in presence of aqueous Ni^{2+}ion rules out any interference from acetate anion as acetate, if present, removed from the reaction medium by the formation of stable $Ni(AcO)_2$ salt. Also, the interference shown by the hydroxyl ion could be neglected as the pH of water is neutral or near neutral (Figure 4.11).
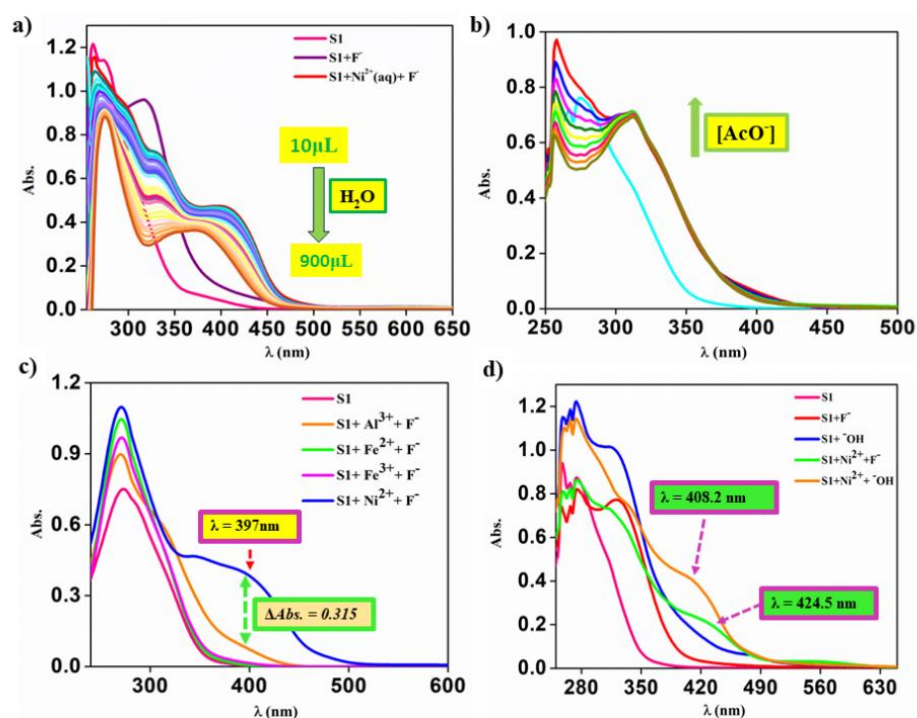

Figure 4.11: (a) UV-Vis spectra of **S1** [6×10^{-5} M] in DMSO in presence of NaF (aq) and Ni^{2+}(aq) upon incremental addition if water; (b) (a) UV-Vis spectra of dilution of **S1** [6×10^{-5} M] in DMSO upon gradual addition of AcO^- ion in presence of Ni(II) ion; (c) Interference study of different metal cation in presence of F^- ion; (d) Interference study of hydroxyl ion in presence of Ni(II) ion.

4.3.4.2. Electrochemical study

To determine whether the probe molecules can serve as electrochemical sensors for aqueous fluoride ions, we investigated the redox behaviour of the probes in the presence of F^- and Ni(II) ions. Cyclic voltammograms (CVs) of **S1** and **S2** were recorded from −2.0 to +1.5 V and −2.0 to +2.0 V, respectively. The CV of **S1** in DMSO displayed a pseudo-

reversible redox couple at −0.53 and −1.11 V. Adding tetrabutylammonium fluoride to the **S1** solution resulted in the emergence of another oxidation peak at 1.27 V (Figure 4.12) whereas addition of NaF (aq) solution did not depict any remarkable change the CV pattern, indicating **S1**'s inefficiency toward fluoride ions in an aqueous medium. A similar observation was noted for **S2** (Figure 4.12 c,d). Conversely, adding aqueous NaF solution to **S1** in the presence of Ni(II) caused significant changes in the CV, revealing two oxidation peaks at −0.57 and 0.41 V and two reduction peaks at −0.81 and −1.62 V (Figure 4.12b). The peaks at Epa = −0.57 V and Epc = −0.81 V correspond to the Ni(II)/Ni(I) and Ni(I)/Ni(II) redox couples, respectively, while the peaks at Epa = 0.41 V and Epc = −1.61 V represent the Ni(III)/Ni(I) and Ni(I)/Ni(III) redox couples, respectively [24-25]. This indicated the in situ Ni(II) complexation of the conjugate base of **S1** formed upon deprotonation by fluoride. Like UV-Vis observation **S2**, did not exhibit any significant response to aqueous sodium fluoride, even in the presence of Ni(II) ion (Figure 4.12c,d) [26-27].
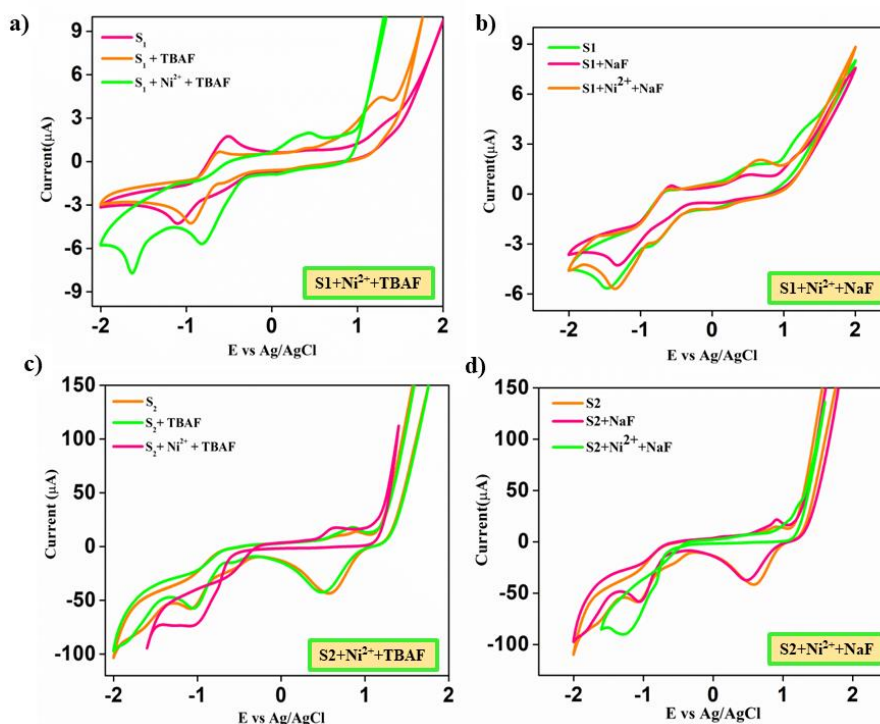

Figure 4.12: (a) Cyclic voltammogram of **S1** (6×10^{-3} M) in presence of TBAF (1×10^{-3} M) and Ni^{2+} (1×10^{-3} M); (b) Cyclic voltammogram of **S1** (6×10^{-3} M) in presence of NaF (1×10^{-3} M) and Ni (1×10^{-3} M) ; (c) Cyclic voltammogram of **S2** (6×10^{-3} M) in presence of TBAF (1×10^{-3} M) and Ni^{2+} (1×10^{-3} M); (d) Cyclic voltammogram of **S2** [6×10^{-3} M] in presence of NaF (1×10^{-3} M) and Ni (1×10^{-3} M).

The electrochemical response of **S1** to incremental additions of aqueous fluoride ions in the presence of Ni(II) was further studied using the differential pulse voltammetry (DPV) technique. The concentrations of **S1** and NiCl$_2$ used for further study were 5×10^{-5} M and 10×10^{-3} M in 40 mL of DMSO, respectively. The DPV was measured in the potential range of 0 to −2.0 V with a modulation amplitude of 10 mV, modulation time of 50 s, steps of −30 mV, and a scan rate of 60 mV/s. The reduction peak at −0.75 V shifted slightly towards the negative potential with a concomitant decrease in the peak current upon incremental addition of aqueous fluoride ions (Figure 4.13a). The change in peak current divilged a linear dependence (Ipc = 0.0062 [NaF] − 0.06552, R^2 = 0.97918) in the concentration range (0-6 ppm) of added fluoride (Figure 4.13b). This linearity suggests that the combination of **S1** and Ni^{2+} ion in DMSO-water medium can be used as an electrochemical probe for the sensing of fluoride ion in water.
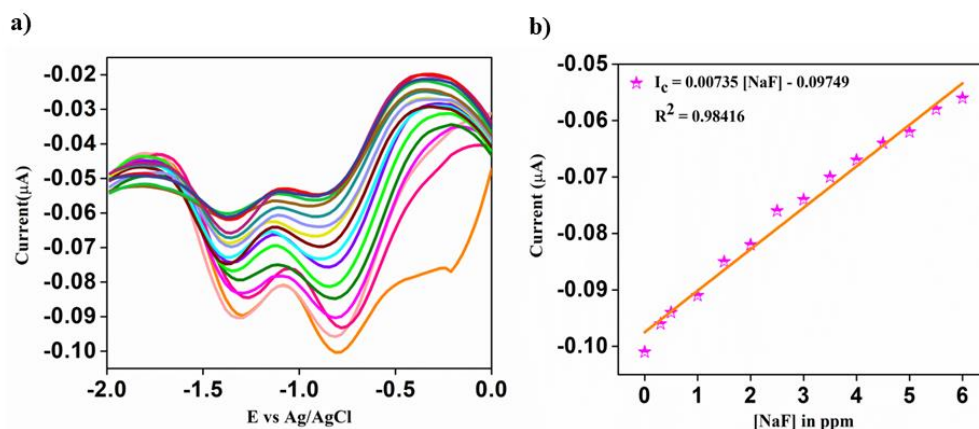

Figure 4.13: (a) Change in the DPV plots of **S1** upon gradual addition of fluoride in presence of Ni (II) salt; (b) The calibration curve of the data for the titration shown in (a). The calculated LOD for electrochemical sensing of fluoride by **S1** in the presence of Ni(II) was found as 0.3 ppm.

4.3.4.3. Investigation of the sensing mechanism

The ^{1}H-NMR titration study conferred that the recognition of fluoride by the probe molecule **S1** involves the Bronsted acid−base deprotonation reaction, which eventually might have led to the creation of favourable coordination sites for Ni(II) complexation. To elucidate the binding pattern of Ni(II) with S1, the metal complex was isolated as a red coloured solid. The FT-IR spectra showed the peaks at 530, 681, and 837 cm^{-1} corresponding to N−Ni−N asymmetric, O−Ni−O asymmetric, and O−Ni−N stretching
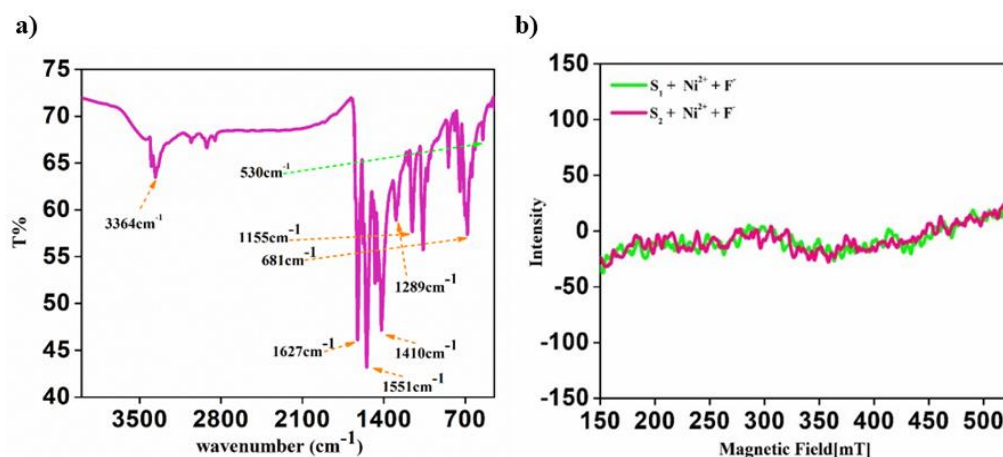
Figure 4.14: (a) FTIR spectra of [NiS1] complex; (b) EPR spectra (100 K, DMSO) [Green: addition of NiCl$_2$ (aq.) to the **S1** solution]; [Pink: addition of NiCl$_2$(aq) to the **S2** solution followed by F$^-$ in DMSO].

vibrations, respectively (Figure 4.14a) [28]. This observation predicted the NiN$_2$O$_2$ coordinating pattern of the [NiS1] complex. Furthermore, to reveal the oxidation state of the Ni(II) species in the reaction medium, an electron spin resonance (ESR) study was performed with the frozen mixture of **S1**, Ni(II) salt, and F$^-$ ions in DMSO medium. ESR spectra revealed the diamagnetic nature of the in situ Ni(II) complex formed during the sensing process (Figure 4.14b) [29,30]. Unfortunately, we did not achieve success in isolating single crystals for the red Ni(II) complex. The UV-Vis, ^{1}H-NMR, FTIR, EPR and electrochemical observation suggest that the in-situ Ni(II) complexation of **S1** reinforcing the fluoride sensing process in aqueous medium (Figure 4.15).
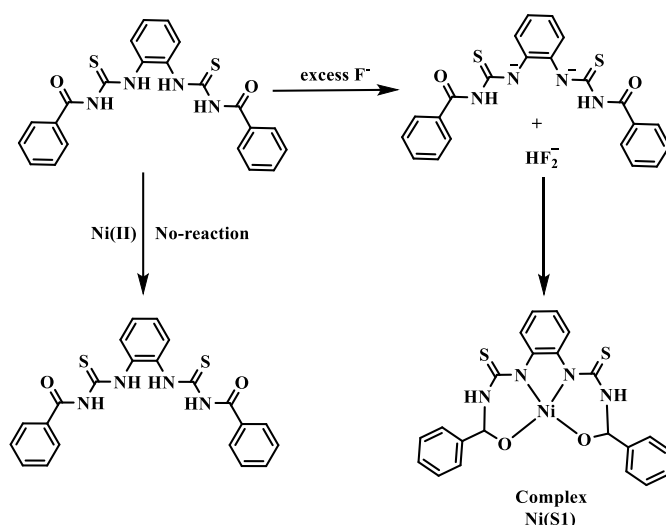

Figure 4.15: Plausible mechanism involved in the process.

4.3.4.4. DFT study

To better understand the structure of the Ni(II) complex and nature of the electronic transitions exhibited by the [NiS1] complex, DFT calculations were performed using the Gaussian 09 package at the WB97XD/6-31++G(d,p) level of theory. The singlet excited state was optimized using time-dependent DFT calculations, considering solvation effects through the inbuilt conductor-like polarizable continuum model in Gaussian 09 [31-34]. The study examined the two possible deprotonation modes of **S1**, finding the more favourable deprotonation at the thiourea N−Hs near the benzoyl group due to the electron-withdrawing nature of the benzoyl group. The optimized structure revealed intramolecular hydrogen bonding interactions between the remaining thiourea N−Hs and the benzoyl moiety. It showed a planar [NiN$_2$O$_2$] η^4-bridging coordination of Ni with the deprotonated thiourea nitrogen and the two benzoyl oxygens. To confirm the presence of Ni−N and Ni−O bonds in the complex, natural bond orbital (NBO) calculations were performed. The HOMO−13 molecular orbital indicated electron densities around the Ni atom, extending over the coordinating N and O atoms, supporting the formation of significant Ni−O and Ni−N bonds with a substantial exchange of electron density among them (Figure 4.16). The computed UV−vis spectrum of [NiS1] closely matched the experimental spectrum, with transitions resulting from HOMO to LUMO. The frontier molecular orbitals derived from the NBO calculations revealed intra ligand charge transfer and ligand-to-metal charge transfer (LMCT) transitions, leading to the observed colorimetric response (Figure 4.17).
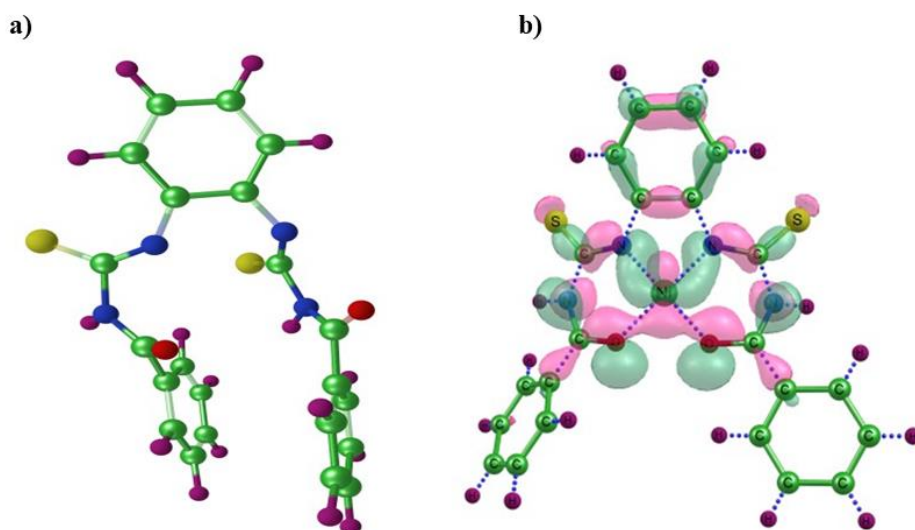

Figure 4.16: (a) DFT optimized structure of deprotonated **S1**; (b) HOMO-13 orbital of [Ni(**S1**)] complex representing the interactions involved.

4-20

The theoretical study also supported that in situ Ni(II) complexation of deprotonated **S1** favours the fluoride-induced deprotonation reaction in an aqueous medium, reinforcing the colorimetric response through favourable LMCT transitions.
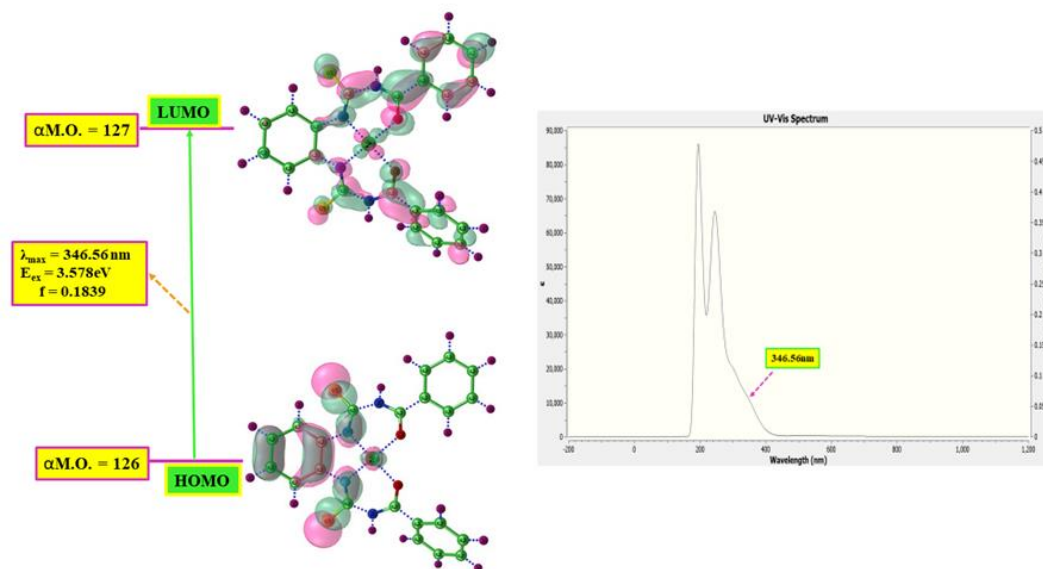

Figure 4.17: Left: Frontier molecular orbitals involved in the UV-Vis absorption of [Ni**S1**]; Right: TDDFT calculated UV-Vis graph of [Ni**S1**].

Further, the predicted IR frequency values for M-N and M-O vibrations matched the experimental values, supporting the accuracy of the predicted structures (Table 4.1).

Group	Experimental Absorption (cm^{-1})	Theoretical Absorption (cm^{-1})
N-H (Stretching)	3364	3627-3632
C=O stretching	1627	1648.90
N-Ni-N rocking	1155	1150
N-Ni-N asymmetric stretching	837	845.54
O-Ni-O asymmetric stretching	681	689
O-Ni-N rocking	530	522

Table 4.2: Comparison of experimental and theoretical IR data.

4.4. Application in Paper Strips

The test strips were created by applying a spot of the probe molecule onto Whatman filter paper. 10 µL of a solution of **S1** (60 µM) in DMSO and 10 µL of an aqueous solution of NiCl2 (10 mM) was put in the paper followed by air-drying for 15 min [35,36]. The test strips were placed on a glass plate, and 10 μL of different concentrations of F^- (0.5, 1, 1.5, 2, 3, 4, 5, 6, 7, and 8 ppm) was added (Figure 4.18). The colour of the spots became yellow with varying intensity upon the addition of fluoridated water, which was clearly discernible with the naked eye. The RGB value of the spots was determined with the RGB colour detector application developed by Raimon Gaspar Fernandez available in the Google play store. The RGB value shows a linear decrease in the percentage of the blue colour index upon the increase in the concentration of fluoride (Figure 4.18).

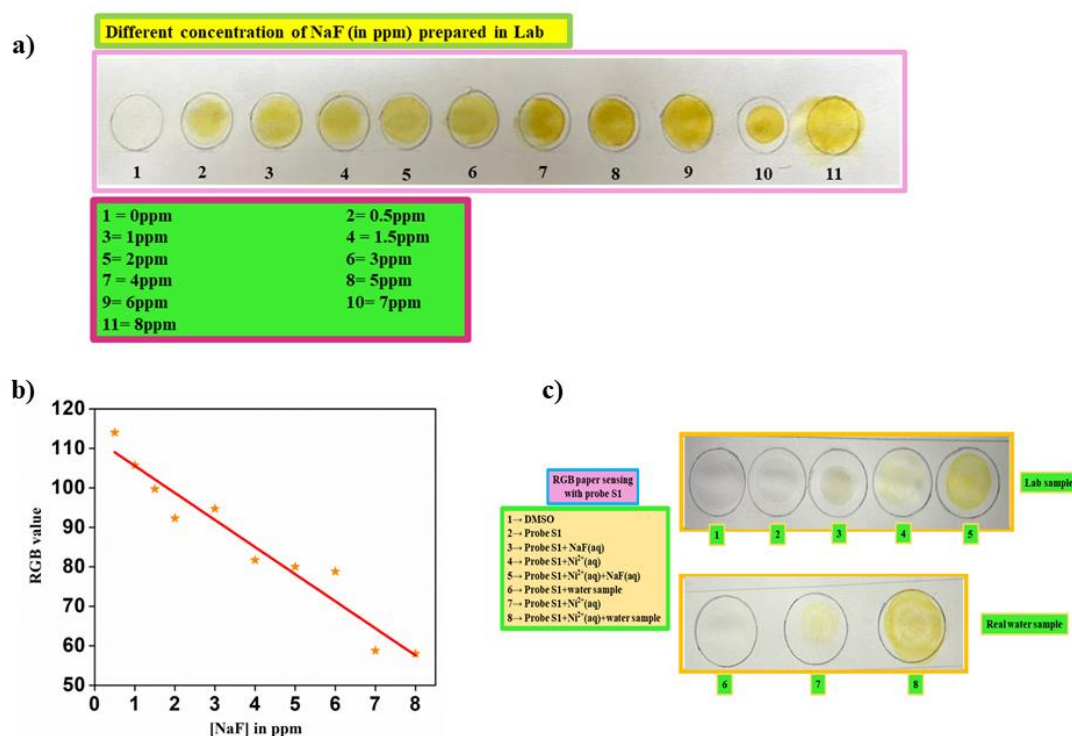**Figure 4.18:** (a) Photograph of the test strips subjected to addition of aqueous solution of F^- (0, 1, 2, 3, 4, 5, 6, 7, 8, 9, 10, 11 ppm) to the circular region having adsorbed **S1** and Ni^{2+}; (b) Decrease in the percentage of the blue colour upon increase in the concentration of fluoride ion; (c) Photograph of the colorimetric change of the test strips upon sequential addition of all the components.

4.5. Validation of the method with real life sample

Finally, as in the previous chapters, we validated the methodology by quantifying the fluoride ion concentration in water samples collected from the Japarajan village, Karbi Anglong district, Assam, India [37,38]. For the analysis, a 3 mL aliquot of 6×10^{-5} M solution of **S1** was placed in a cuvette, to which 50 µL of 10×10^{-3} M $NiCl_2$ in an aqueous medium was added. Subsequently, 50 µL of the water sample was introduced into the mixture. The resultant colorimetric response was analysed using a UV-Vis spectrometer, and the absorbance at a wavelength of 360 nm was measured. Similarly for differential pulse voltammetry (DPV), a 30 mL aliquot of a 1×10^{-3} M solution of **S1** was placed in a beaker, to which 200 µL of a 1×10^{-3} M NiCl2 solution in an aqueous medium was added. Subsequently, 100 µL of the water sample was introduced into the mixture and observed the representative colorimetric change from colourless to yellow, indicating the presence
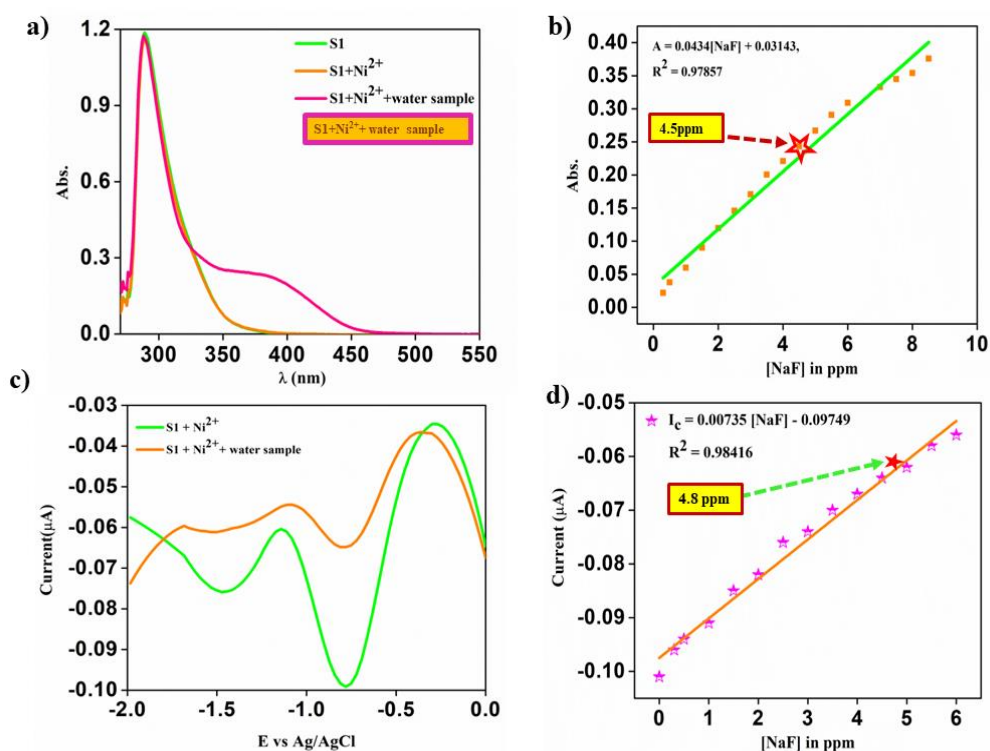
Figure 4.19: (a) UV-Vis spectra of **S1** [6 µM] in DMSO with water sample collected from fluoride affected areas in presence of aqueous Ni^{2+} ion [10 mM]; (b) Calibration curve where star indicates the concentration of fluoride in water sample; (c) DPV of **S1** with water sample collected from fluoride affected areas in presence of aqueous Ni^{2+} ion [1 mM]; (d) Calibration curve where star indicates the concentration of fluoride in water sample.

of fluoride ions. The concentration of fluoride ions was calculated from the calibration curve and determined to be 4.5 ppm (Figure 4.19). Furthermore, the DPV study showed a change in the peak current after adding the water sample, revealing the presence of 4.8 ppm of fluoride ions in the water sample. The results were in good agreement with the concentration obtained from the ion-selective electrode (ISE) measurement, which was found to be 5 ppm. The discrepancy between our methodology and the ISE measurement might be due to interference from other ions present in the sample. This observation clearly demonstrates that the presented methodology can qualitatively and quantitatively determine the presence of fluoride ions in an aqueous medium.

4.6. Conclusion

In conclusion both *bis*-thiourea probe molecules **S1** and **S2** exhibited a colorimetric response towards fluoride (F^-) and acetate (AcO^-) ions in DMSO medium. However, neither **S1** nor **S2** showed any affinity for fluoride ion in aqueous medium. Interestingly **S1** selectively senses inorganic fluoride ion in water when Ni (II) ions are present in the reaction medium. The methodology for detecting aqueous fluoride ions with **S1** has been validated through UV-Vis spectroscopy and DPV methods. The LODs calculated by UV−vis spectroscopy and DPV techniques are 0.2 and 0.3 ppm respectively, well below the WHO limit set for fluoride in drinking water. The methodology was also successfully demonstrated in cellulose paper strip platform. The methodology was finally tested with environmental samples, and the results corroborated well with the ISE data. The work is going on to enrich the methodology toward more impactful application in routine monitoring of fluoride ions in drinking water.

4.7. References:

[1]   Jose, D. A., Kumar, D. K., Ganguly, B., and Das, A. Efficient and simple colorimetric fluoride ion sensor based on receptors having urea and thiourea binding sites. *Organic letters*, 6(20):3445-3448, 2004.

[2]   Li, Z. Y., Su, H. K., Tong, H. X., Yin, Y., Xiao, T., Sun, X. Q., and Wang, L. Calix [4] arene containing thiourea and coumarin functionality as highly selective fluorescent and colorimetric chemosensor for fluoride ion. *Spectrochimica Acta Part A: Molecular and Biomolecular Spectroscopy*, 200:307-312, 2018.

[3]   Kim, D. W. Anion Sensing Properties of New Colorimetric Chemosensors Based on Thiourea and Urea Moieties. *Bulletin of the Korean Chemical Society*, 33(12):4280-4280, 2012.

[4]   Li, S., Cao, X., Chen, C., and Ke, S. Novel salicylic acid-oriented thiourea-type receptors as colorimetric chemosensor: synthesis, characterizations and selective naked-eye recognition properties. *Spectrochimica Acta Part A: Molecular and Biomolecular Spectroscopy*, 96:18-23, 2012.

[5]   Han, F., Bao, Y., Yang, Z., Fyles, T. M., Zhao, J., Peng, X., and Sun, S. Simple bisthiocarbonohydrazones as sensitive, selective, colorimetric, and switch-on fluorescent chemosensors for fluoride anions. *Chemistry–A European Journal*, 13(10):2880-2892, 2007.

[6]   Misra, A., Shahid, M., and Dwivedi, P. An efficient thiourea-based colorimetric chemosensor for naked-eye recognition of fluoride and acetate anions: UV–vis and 1HNMR studies. *Talanta*, 80(2):532-538, 2009.

[7]   Veale, E. B., and Gunnlaugsson, T. Bidirectional photoinduced electron-transfer quenching is observed in 4-amino-1, 8-naphthalimide-based fluorescent anion sensors. *The Journal of Organic Chemistry*, 73(20):8073-8076, 2008.

[8]   Raposo, M. M. M., Garcia-Acosta, B., Abalos, T., Calero, P., Martinez-Manez, R., Ros-Lis, J. V., and Soto, J. Synthesis and study of the use of heterocyclic thiosemicarbazones as signaling scaffolding for the recognition of anions. *The Journal of Organic Chemistry*, 75(9):2922-2933, 2010.

[9]   Lee, J. Y., Cho, E. J., Mukamel, S., and Nam, K. C. Efficient fluoride-selective fluorescent host: experiment and theory. *The Journal of organic chemistry*, 69(3):943-950, 2004.

[10]   Cho, E. J., Ryu, B. J., Lee, Y. J., and Nam, K. C. Visible colorimetric fluoride ion sensors. *Organic letters*, 7(13):2607-2609, 2005.

[11]   Jose, D. A., Kumar, D. K., Ganguly, B., and Das, A. Efficient and simple colorimetric fluoride ion sensor based on receptors having urea and thiourea binding sites. *Organic letters*, 6(20):3445-3448, 2004.

[12] Hu, Z. Q., Cui, C. L., Lu, H. Y., Ding, L., and Yang, X. D. A highly selective fluorescent chemosensor for fluoride based on an anthracene diamine derivative incorporating indole. *Sensors and Actuators B: Chemical*, 141(1):200-204, 2009.

[13] Yong, X., Wan, W., Su, M., You, W., Lu, X., Yan, Y., and Masuda, T. Thiourea-functionalized poly (phenyleneethynylene): fluorescent chemosensors for anions and cations. *Polymer Chemistry*, 4(15):4126-4133, 2013.

[14] Razak, N. H. A., Tan, L. L., Hasbullah, S. A., and Heng, L. Y. Reflectance chemosensor based on bis-thiourea derivative as ionophore for copper (II) ion detection. *Microchemical Journal*, 153:104460, 2020.

[15] Liu, Y., Yang, L., Li, L., Liang, X., Li, S., and Fu, Y. A dual thiourea-appended perylenebisimide "turn-on" fluorescent chemosensor with high selectivity and sensitivity for Hg^{2+} in living cells. *Spectrochimica Acta Part A: Molecular and Biomolecular Spectroscopy*, 241:118678, 2020.

[16] Lee, J. Y., Rao, B. A., Hwang, J. Y., and Son, Y. A. A novel sensing capabilities and structural modification from thiourea to urea derivative by Hg $(ClO_4)_2$: Selective dual chemodosimeter for Hg^{2+} and F^- ions. *Sensors and Actuators B: Chemical*, 220:1070-1085, 2015.

[17] Kundu, S., Egboluche, T. K., Yousuf, Z., and Hossain, M. A. Spectroscopic and colorimetric studies for anions with a new urea-based molecular cleft. *Chemosensors*, 9(10):287, 2021.

[18] Russ, T. H., Pramanik, A., Khansari, M. E., Wong, B. M., and Hossain, A. A quinoline based bis-urea receptor for anions: A selective receptor for hydrogen sulfate. *Natural Product Communications*, 7(3):1934578X1200700307, 2012.

[19] Manna, U., Portis, B., Egboluche, T. K., Nafis, M., and Hossain, M. A. Anion binding studies of urea and thiourea functionalized molecular clefts. *Frontiers in Chemistry*, 8:575701, 2021.

[20] Ghosh, K., Sarkar, A. R., and Masanta, G. An anthracene based bispyridinium amide receptor for selective sensing of anions. *Tetrahedron Letters*, 48(49):8725-8729, 2007.

[21] Kundu, S., Egboluche, T. K., Yousuf, Z., and Hossain, M. A. Spectroscopic and colorimetric studies for anions with a new urea-based molecular cleft. *Chemosensors*, 9(10):287, 2021.

[22] Zhang, Y., and Jiang, S. Fluoride-responsive gelator and colorimetric sensor based on simple and easy-to-prepare cyano-substituted amide. *Organic & Biomolecular Chemistry*, 10(34):6973-6979, 2012.

[23] Benesi, H. A., and Hildebrand, J. H. J. A spectrophotometric investigation of the interaction of iodine with aromatic hydrocarbons. *J. Am. Chem. Soc.,* 71 (8):2703−2707, 1949

[24] Armbruster, D. A., and Pry, T. Limit of blank, limit of detection and limit of quantitation. *The clinical biochemist reviews*, 29(Suppl 1):S49, 2008.

[25] Zhang, Y. C., Chilukuri, B., Hanson, T. B., Heiden, Z. M., and Lee, D. Y. Connecting Solution-Phase to Single-Molecule Properties of Ni (Salophen). *The Journal of Physical Chemistry Letters*, 10(13): 3525-3530, 2019.

[26] Tang, H. M., and Fan, W. Y. Dithiolato-Bridged Nickel (II) Salicylcysteamine Complexes as Robust Proton Reduction Electrocatalysts: Cyclic Voltammetry and Computational Studies. *Inorganic Chemistry*, 60(23):17933-17941, 2021.

[27] Maity, D., Bhaumik, C., Mondal, D. and Baitalik, S. Ru (II) and Os (II) complexes based on terpyridyl-imidazole ligand rigidly linked to pyrene: synthesis, structure, photophysics, electrochemistry, and anion-sensing studies. *Inorganic Chemistry*, 52(24):13941-13955, 2013.

[28] Nakamoto, K. Applications in coordination, organometallic, and bioinorganic chemistry. 1997.

[29] Dhawan, S., Devnani, H., Babu, J., Singh, H., Haider, M. A., Khan, T. S., and Haridas, V.Supersensitive detection of anions in pure organic and aqueous media by amino acid conjugated Ellman's reagent. *ACS Applied Bio Materials*, 4(3):2453-2464, 2021.

[30] Meron, S., Shenberger, Y., and Ruthstein, S. The advantages of EPR spectroscopy in exploring diamagnetic metal ion binding and transfer mechanisms in biological systems. *Magnetochemistry*, 8(1):3, 2021.

[31] Ammeter, J. H. EPR of orbitally degenerate sandwich compounds. *Journal of Magnetic Resonance (1969)*, 30(2):299-325, 1978.

[32] Frisch, M. E., Trucks, G. W., Schlegel, H. B., Scuseria, G. E., Robb, M. A., Cheeseman, J. R., and Fox, D. J. *Gaussian 16, Revision C.01*; Gaussian, Inc.: Wallingford, CT, 2016.

[33] Adamo, C., and Jacquemin, D. The calculations of excited-state properties with Time-Dependent Density Functional Theory. *Chemical Society Reviews*, 42(3):845-856, 2013

[34] Takano, Y., and Houk, K. N. Benchmarking the conductor-like polarizable continuum model (CPCM) for aqueous solvation free energies of neutral and ionic organic molecules. *Journal of Chemical Theory and Computation*, 1(1):70-77, 2005.

[35] Mahishi, A. A., Shet, S. M., Mane, P. V., Yu, J., Sowriraajan, A. V., Kigga, M., and Kurkuri, M. D. Ratiometric colorimetric detection of fluoride ions using a schiff base sensor: enhancing selectivity and sensitivity for naked-eye analysis. *Analytical Methods*, 15(26):3259-3267, 2023.

[36] Wu, X., Wang, H., Yang, S., Tian, H., Liu, Y., and Sun, B. Highly sensitive ratiometric fluorescent paper sensors for the detection of fluoride ions. *ACS omega*, 4(3):4918-4926, 2019.

[37] Puzari, A., Khan, P., Thakur, D., Kumar, M., Shanu, K., and Chutia, P. Quality assessment of drinking water from Dimapur District of Nagaland and Karbi-Anglong District of Assam for possible related health hazards. *Current World Environment*, 10(2):634, 2015.